RSC Advances

PAPER

View Article Online
View Journal | View Issue

Cite this: *RSC Adv.*, 2020, **10**, 25639

Tunable magnetic textures and excitation modes in FePt multilayer films

Mei Bi,[a] *[a] Le Yuan,[ab] Xin Wang,[b] Xiaolong Weng[b] and Longjiang Deng[b]

Micromagnetic simulations have been performed to investigate the magnetic textures and dynamic properties of FePt-based multilayer films. The uniform state, Neel skyrmion and Bloch skyrmion can be obtained using variable magnetic parameters. A microwave field is applied to induce spin precession along the out-plane and in-plane axes. For the perpendicular resonance modes, low-frequency peaks are identified as domain-wall modes. It is shown that radial-like and azimuthal-like resonance modes appear with increase in frequency. The excited modes are qualitatively different when the microwave field is applied along the in-plane axis. For the uniform state, the phase responds to the excitation with waves that spread out in a circle, which is a characteristic feature of the azimuthal mode in the spin wave. Because of the nonuniform effective field in Neel and Bloch skyrmions, the dynamic response localizes at the center and the edge spreads into the adjacent domains. These observations are important for tunable and abundant high-frequency magnetic properties in skyrmion-based devices.

Received 19th March 2020
Accepted 22nd June 2020

DOI: 10.1039/d0ra02534h

rsc.li/rsc-advances

Introduction

Unconventional spin-electronic phenomena have attracted considerable interest due to their novel physical properties and potential applications.[1–7] Specifically, a skyrmion is a topological spin texture that is observed in non-centrosymmetric chiral crystals and heavy metal/ultrathin ferromagnetic layers with relatively weak Dzyaloshinskii–Moriya interactions (DMI).[8–11] Rather than DMI, skyrmion crystals are stabilized at room temperature *via* interlayer exchange coupling between patterned structures with soft magnetic properties and out-of-plane magnetized films.[12–17] This class of skyrmion structures overcome the obstacles faced by DMI, which cannot support the stable presence of the magnetic skyrmion lattice at room temperature without an appropriate magnetic field.[12] Initially, the skyrmion crystals were realized by a simulated structure, which is composed of a magnetic film with a perpendicular anisotropy and magnetic disks with a vortices spin texture.[13] Experimentally, the existence of the artificial skyrmion was confirmed by element-specific X-ray magnetic circular dichroism measurements, magnetic force microscopy, and Kerr microscopy imaging.[14–16] Patterned films with perpendicular anisotropy are proposed to create 2D skyrmion lattices in the absence of DMI.[17] By adjusting magnetic parameters, different stable skyrmion lattices can be obtained and the lattices can be switched. Furthermore, the skyrmion helicity can be changed by adjusting the geometry of the patterned elements and applying a magnetic field. The advantage of this approach is that the artificial magnetic skyrmions are more stable than conventional magnetic materials at room temperature. Skyrmionic states can then be easily controlled by tailoring the geometry and magnetic parameters.

Recently, the dynamic excitations of the nonuniform spin structure in patterned magnetic skyrmions were investigated.[18–27] Theoretical calculations demonstrate that the breathing modes are mediated by geometrically quantized spin waves.[21] The dynamic mechanisms are completely different from those of uniformly magnetized system reversals. Using an in-plane external microwave magnetic field, the excited modes were confirmed as both counterclockwise (CCW) and clockwise (CW) modes. With an out-plane external field, the excited mode was the breathing mode.[22,23] The various resonant modes depend on the spin structure and the influence of magnetic field excitation. This suggests that designing the spin texture would be a promising approach to control the resonance frequency and mode. In this letter, we focus on an isolated skyrmion in a nanostructured FePt multilayer to realize tunable magnetic textures and investigate the dynamic effects that can be retrieved from this engineered state. Complex non-linear resonant excitations of topological objects in FePt multilayer films have seldom been reported and the associated physical mechanism remains unclear. FePt films have variable magnetocrystalline anisotropy due to the partial chemically ordered phase. The fabrication and magnetic behavior of the anisotropy-modulated FePt films have been described in detail elsewhere.[28] Gradual changes in the strength of the magnetic anisotropy and

[a]*Key Laboratory of Fluid and Power Machinery of Ministry of Education, School of Materials Science and Engineering, Xihua University, Chengdu 610039, China. E-mail: meibi0323@163.com; Fax: +86-28-8772-9250; Tel: +86-28-8772-9250*

[b]*National Engineering Research Center of Electromagnetic Radiation Control Materials, University of Electronic Science and Technology of China, Chengdu 610054, China*

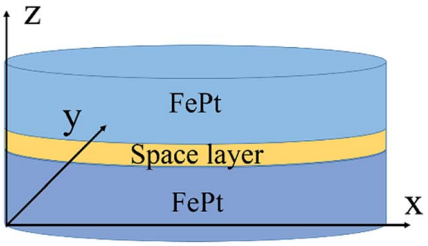

Fig. 1 Schematic of the FePt multilayer films.

the exchange interactions between the multilayer films led to continuous phase transitions between different stable magnetic configurations. By adjusting the magnetic parameters of the FePt film in the top and bottom layers, the magnetic skyrmion textures shift from the Neel skyrmion to the Bloch skyrmion. We confirm that the complex spin structures of the proposed FePt multilayer films can enrich the microwave characteristics of magnetic materials. The corresponding excitations, activated by a microwave magnetic field, will contribute to the understanding and manipulation of skyrmions for various applications.

Methods

A schematic of the structure of a FePt multilayer film is illustrated in Fig. 1. Nanodisks with two FePt layers and a non-magnetic (NM) space layer are proposed to investigate the formation and the dynamics of magnetic skyrmion in the absence of DMI by a OOMMF code based on the Landau–Lifshitz–Gilbert equation.[29] The top and bottom FePt layers are exchange coupled with exchange stiffness of $A = 1.1 \times 10^{-11}$ J m^{-1}, an adjustability value of the saturation magnetization and the magnetic anisotropy constant. All of the parameters were the same in our experimental system and in line with the theoretical calculation: a saturation magnetization of $M_s = 6.9 \times 10^5$ A m^{-1}, 8.6×10^5 A m^{-1} or 1.4×10^6 A m^{-1}; an out-plane magnetic anisotropy of the bottom FePt film fixed at $k_l = 4 \times 10^5$ J m^{-3} and the top FePt film in the range of 0–5.4 $\times$ 10^5 J m^{-3} (k_u); FePt film with a diameter of $D = 200$ nm; top FePt film with a thickness of $t_u = 20$ nm and the bottom FePt film with a thickness of $t_l = 10$ nm; a space layer thickness of $t_s < 2$ nm. The models were then calculated with a cell size of 2 nm $\times$ 2 nm $\times$ 1 nm. For the static magnetic configuration, dimensionless damping of $\alpha = 0.5$ was selected to obtain a rapid convergence. The model was excited by an external microwave field along the in-plane and out-plane axes. To improve the accuracy of the resonance peaks, we assumed that $\alpha = 0.01$ in the dynamic simulation. For the calculation, the LLG equation was solved with a difference method and a Runge–Kutta method.

Results and discussions

Variable spin textures result in different magnetic parameters. The saturation magnetization and magnetic anisotropy constants used in the experiments are summarized in Table 1. Using these magnetic parameters, micromagnetic simulations present different skyrmion states in the absence of DMI and an external magnetic field (shown in Fig. 2(a)). The arrows represent the spin orientation at each cell of the simulated sample. According to the magnetic parameters shown in Table 1, the system evolves in the following sequence: the uniform state, Neel skyrmion, and Bloch skyrmion. For the uniform state, the distribution of the preferred orientation of the moments in the ground state is approximately along z direction and results in a perpendicularly magnetized single domain. More precisely, the magnetization is uniformly magnetized along the out-plane direction in the region near the center of the FePt multilayer films. However, the spins present a slightly tilted angle at the edges because of the competition between demagnetization and exchange energy. The magnetization rotates in the domain wall perpendicular to the radial direction in the Bloch skyrmion. The main difference is that for decreasing magnetic anisotropy and increasing saturation magnetization, the vortex-like state is more stable. However, it rotates along the in-plane radial

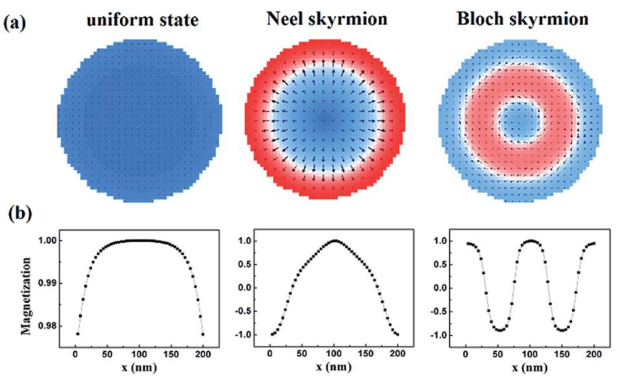

Fig. 2 (a) Evolution of the spin texture as a function of the magnetic parameters. From left to right, the spin texture represents the uniform state, Neel skyrmion, and Bloch skyrmion. The color denotes the spin component along the z direction, while the arrows represent the spin direction. (b) The corresponding magnetization component m_z along the nanodisk diameter ($y = 100$ nm).

Table 1 List of magnetic parameters of the FePt films

	The uniform state		Neel skyrmion		Bloch skyrmion	
Magnetic parameters	Top layer	Bottom layer	Top layer	Bottom layer	Top layer	Bottom layer
M_s (A m^{-1})	6.9×10^5	6.9×10^5	1.4×10^6	1.4×10^6	8.6×10^5	6.9×10^5
k (J m^{-3})	5.4×10^5	4×10^5	4×10^5	4×10^5	0	4×10^5

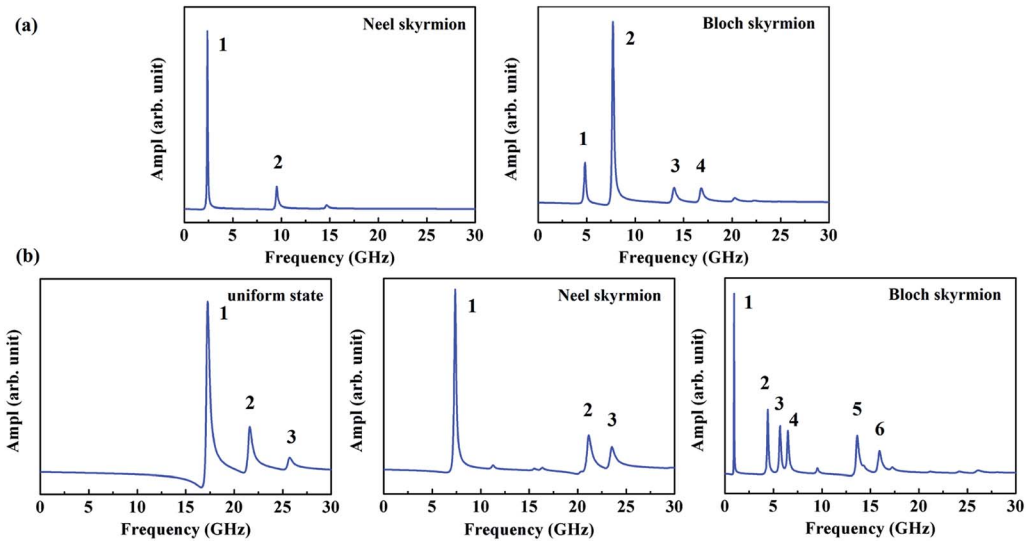

Fig. 3 Imaginary parts of the (a) out-of-plane and (b) in-plane dynamical susceptibilities. Upper panel: magnetic excitation spectra of Neel skyrmion, and Bloch skyrmion activated by the out-of-plane microwave magnetic field. Lower panel: magnetic excitation spectra of the uniform state, Neel skyrmion, and Bloch skyrmion activated by the in-plane microwave magnetic field.

direction in the Neel skyrmion. It was observed that the diameter of the skyrmion is directly proportional to the magnetic anisotropy. In Fig. 2(b), we present a line scan of the perpendicular (m_z) component of the magnetization in the FePt multilayer films with a uniform state, Neel skyrmion state, and Bloch skyrmion state. It is well known that the spin configuration prefers out-plane magnetization when the nanodots possess strong perpendicular magnetic anisotropy. Therefore, the magnetic moment tends towards uniform distribution when the magnetic anisotropy is large. As the magnetic anisotropy decreases, the spins switch to all directions in the Neel and Bloch skyrmions, which can be seen in the m_z magnetization profile.

Fig. 3 shows the resonance absorption spectra simulated for the FePt multilayer films with different spin textures. A microwave field was applied along the z-direction (Fig. 3(a)) and x-direction (Fig. 3(a)). In the simulated results, entirely different microwave properties are observed in the skyrmion texture. Four distinct resonance modes are observed for the out-plane applied field in Bloch skyrmion and are located at 4.83 GHz, 7.71 GHz, 14.01 GHz, and 16.82 GHz. The frequency-domain profile of the out-of-plane microwave perturbation reveals that there are two peaks in Neel skyrmion at 2.37 and 9.5 GHz (shown in Fig. 3(a)). In Fig. 3(b), by applying an external field along the in-plane direction of the FePt multilayer films, we observe more complex magnetization dynamics for all of the simulated samples. For the uniform state, the high-frequency peaks are in-plane modes, which can only be found when the field is applied along the in-plane axis. This is due to the uniform distribution of magnetization along the z axis. The main dynamic behavior exhibited in Neel skyrmion is left-shifted frequencies compared to the uniform state. The peak with the highest intensity is red-shifted to 7.35 GHz, while the other two lower peaks are shifted to >20 GHz. For Bloch skyrmion, six peaks are observed and the main peaks are very sharp without splitting. The absorption peaks have high intensities and relatively low intensities, which exhibit red and blue shifts, respectively. The resonance peaks located between 4.4 and 6.5 GHz are arranged very close to each other. Moreover, two more absorption peaks with slightly lower intensities are

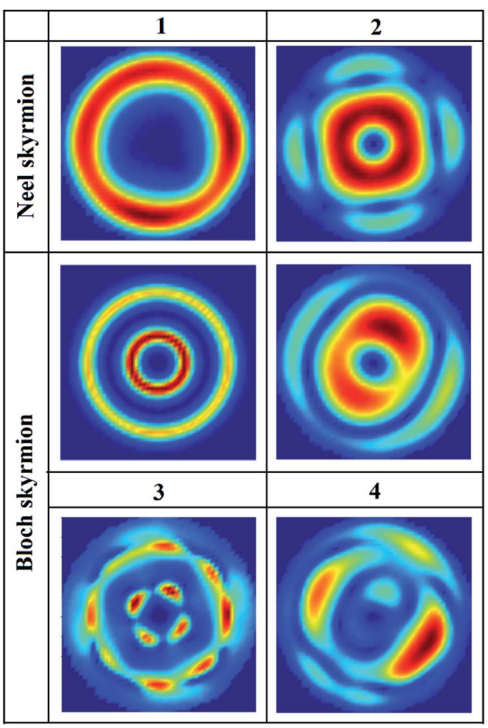

Fig. 4 Dynamic response of the different magnetic textures corresponding to the marked locations in Fig. 3(a) for Neel skyrmion and Bloch skyrmion.

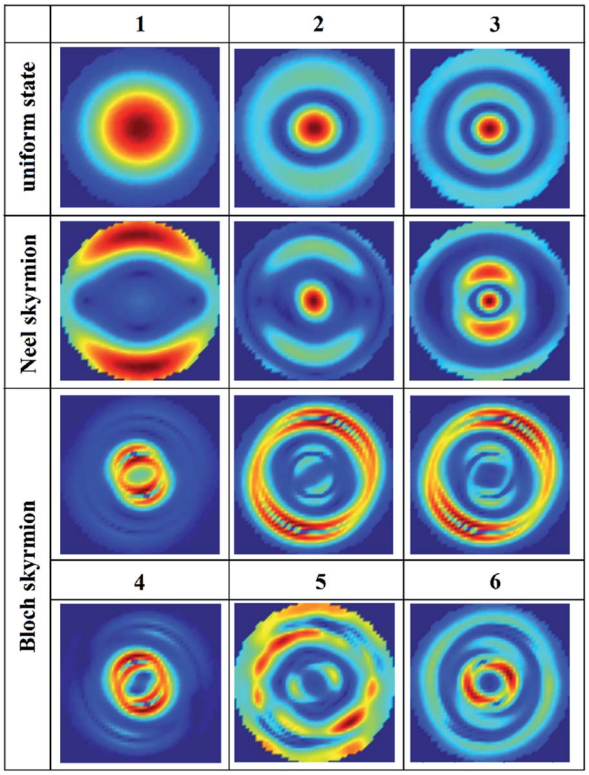

Fig. 5 The dynamic response of the different magnetic textures corresponding to the marked locations in Fig. 3(b) for the uniform state, Neel skyrmion and Bloch skyrmion.

observed at 13 GHz. Note that the highest peak appears in the lowest resonant frequency and the peak intensity gradually decreases as the frequency increases for the in-plane dynamical excitation.

To study the resonance modes, we performed a discrete-time Fourier transform (DTFT) at the absorption frequency in the x–y plane. The distribution of the dynamic m_z under the out-plane field excitation are shown in Fig. 4. The resonant absorbing intensities are represented by different colors. Unlike blue, which represents the resonance areas of weak intensities, red indicates the max absolute value. It is observed that domain-wall (DW) resonances exist in two types of skyrmion at the lowest frequencies (mode 1) of the excitation spectra. The local spin and location of the domain wall are clearly reported in Fig. 2. The domain wall acts as an interface separating the magnetic domains, which are represented by white. Note that the static magnetization parallel to the longitudinal excitation is not discussed further.

As the magnetic field is perpendicular to the direction of the magnetic moment, resonance can occur. The excited states in mode 2 of Neel skyrmion and Bloch skyrmion are considered radial-like modes, which possess the characteristics of the confined spin-wave mode around the skyrmion. Mode 4 in Bloch skyrmion is an azimuthal-like mode, appearing within the inhomogeneous spots, which is separated by the nodes mixed with nonzero magnetization.

Table 2 Overview and parameters of selected skyrmion-based materials

Material	D (mJ m^{-2})	Magnetic state	Frequency (GHz)	Reference
CoFe–MgO	0–2	Vortex/skyrmion	0–5.5	32 and 33
FeGe	1.58	Skyrmion	0–25	31
Co/Ru/Co	0	Skyrmion	0–5	34
FePt/NM/FePt	0	Uniform/skyrmion	0–26	—

Simultaneous radial-like and azimuthal-like modes are observed in mode 3. The radial modes feature a phase change perpendicular to the direction of the radius, while the phase in the azimuthal modes tends to vary around the center of the nanodisk. The computed dynamic maps of local susceptibility, associated with the multilayer films by applying an in-plane magnetic field, are reported in Fig. 5. For the uniform state, three peaks are identified as the appearance of the radial spin-wave resonance. The radial spin-wave modes can be analyzed by a quantized number, which reflects the number of the wave-function node and corresponding frequencies. For Neel skyrmion, the resonance intensity in mode 1 is obviously suppressed at the center of the FePt multilayer films. Absorption occurred in the region along the edge in the form of a two dimensional shell. It is evident from mode 2 and 3 that the intensity of the shell-like edge mode is gradually weakened, while the center mode is obviously enhanced with increasing frequency. For modes 2, 3, and 5 in Neel skyrmion, the strongest excitation appears at the dot edges; however, a weak component is observed around the core. Nevertheless, the dynamic response in modes 1, 4, and 6 are primarily localized in the central region.

Similar dynamic properties of magnetic skyrmions were reported in chiral magnets and helimagnetic nanostructures, where topological spin distribution was induced by Dzyaloshinskii–Moriya interactions[30,31] (see Table 2 for the list of materials.) Because of interfacial DMI, low-frequency eigenmodes and the high-frequency spin-wave modes in the skyrmion states can be observed in the excitation spectrum. The change in the DMI exchange interaction constant (D) leads to magnetic phase transitions between different stable magnetic configurations. Despite the absence of Dzyaloshinskii–Moriya interactions, the FePt multilayer film shows a spontaneous skyrmion texture. This allows for mapping of the dynamic resonance modes and leads to an understanding of the rich dynamic properties of skyrmion without the requirement for an external magnetic field or a lower temperature. By designing magnetic and geometric parameters, it is possible to obtain different stable magnetic skyrmions and stimulate non-generic dynamic magnetic responses.

Conclusions

In summary, we consider the influence of the magnetic parameters of top and bottom FePt films on the dynamic

properties of skyrmions. The uniform state, Neel skyrmion, and Bloch skyrmion are obtained at a given saturation magnetization and magnetic anisotropy. Microwave field excitation is then applied to investigate spin dynamics. After perturbation, the dynamic simulation results are calculated in the time domain of the magnetization in each cell. Discrete-time Fast Fourier Transform (FFT) processing was performed to obtain the excitation spectrum, which indicates the response results. To study the dynamic response, we further simulated the snapshot of dynamical magnetization for all of the resonant modes. The domain-wall mode was observed at the lowest frequency, while extensive spin-wave modes at higher frequencies are observed in the dynamic response along the perpendicular direction. With the in-plane microwave field, the uniform state shows three resonance peaks, which correspond to the radial spin-wave modes. Neel skyrmion and Bloch skyrmion present a more complicated picture of the dynamics because of inhomogeneous magnetization. For the existence of the disordered A phase (with a random distribution of the Fe and Pt atoms in the cubic cell) and ordered $L1_0$ phase (with a chemical ordered fct structure) in the FePt films, the perpendicular anisotropy can be effectively controlled by a deposition process. In addition, varying the magnetic parameters can result in the nucleation and annihilation of different magnetic structures. In this letter, the uniform state and different skyrmion states are presented as examples to illustrate this phenomenon. Thus, it should be feasible to experimentally realize the proposed design of skyrmion formation and excitation, which may lead to further tailoring of the magnetic textures for applications such as microwave filters and waveguide structures.

Conflicts of interest

There are no conflicts to declare.

Acknowledgements

This work was supported by the NSFC (Grant No. 51902269 and Grant No. 51972276), the research was supported by "Young Scholars Reserve Talents" program of Xihua University and Scientific Research Project of Sanya (2014CZ12).

References

1 X. Zhang, Y. Zhou, K. M. Song, T.-E. Park, J. Xia, M. Ezawa, X. Liu, W. Zhao, G. Zhao and S. Woo, *J. Phys.: Condens. Matter*, 2020, **14**, 32.
2 K.-W. Moon, J. Yoon, C. Kim and C. Hwang, *Phys. Rev. Appl.*, 2019, **6**, 12.
3 T. Nozaki, Y. Jibiki, M. Goto, E. Tamura, T. Nozaki, H. Kubota, A. Fukushima, S. Yuasa and Y. Suzuki, *Appl. Phys. Lett.*, 2019, **1**, 114.
4 C. Kind, S. Friedemann and D. Read, *Appl. Phys. Lett.*, 2020, **2**, 116.
5 Q. Mahmood, M. Hassan, S. H. A. Ahmad, K. C. Bhamu, A. Mahmood and S. M. Ramay, *J. Phys. Chem. Solids*, 2019, **128**, 283–290.
6 Q. Mahmood, M. Hassan, S. H. A. Ahmad, A. Shahid and A. Laref, *J. Phys. Chem. Solids*, 2018, **120**, 87–95.
7 H. A. Qayyum, M. F. Al-Kuhaili, S. M. A. Durrani, T. Hussain, S. H. A. Ahmad and M. Ikram, *J. Alloys Compd.*, 2018, **747**, 374–384.
8 S. Muhlbauer, B. Binz, F. Jonietz, C. Pfleiderer, A. Rosch, A. Neubauer, R. Georgii and P. Boni, *Science*, 2009, **323**, 915–919.
9 X. Z. Yu, Y. Onose, N. Kanazawa, J. H. Park, J. H. Han, Y. Matsui, N. Nagaosa and Y. Tokura, *Nature*, 2010, **465**, 901–904.
10 W. J. Jiang, P. Upadhyaya, W. Zhang, G. Q. Yu, M. B. Jungfleisch, F. Y. Fradin, J. E. Pearson, Y. Tserkovnyak, K. L. Wang, O. Heinonen, S. G. E. te Velthuis and A. Hoffmann, *Science*, 2015, **349**, 283–286.
11 S. Heinze, K. von Bergmann, M. Menzel, J. Brede, A. Kubetzka, R. Wiesendanger, G. Bihlmayer and S. Blugel, *Nat. Phys.*, 2011, **7**, 713–718.
12 N. Nagaosa and Y. Tokura, *Nat. Nanotechnol.*, 2013, **8**, 899–911.
13 L. Sun, R. X. Cao, B. F. Miao, Z. Feng, B. You, D. Wu, W. Zhang, A. Hu and H. F. Ding, *Phys. Rev. Lett.*, 2013, **110**, 167201.
14 J. Li, A. Tan, K. W. Moon, A. Doran, M. A. Marcus, A. T. Young, E. Arenholz, S. Ma, R. F. Yang, C. Hwang and Z. Q. Qiu, *Nat. Commun.*, 2014, **5**, 4704.
15 B. F. Miao, L. Sun, Y. W. Wu, X. D. Tao, X. Xiong, Y. Wen, R. X. Cao, P. Wang, D. Wu, Q. F. Zhan, B. You, J. Du, R. W. Li and H. F. Ding, *Phys. Rev. B: Condens. Matter Mater. Phys.*, 2014, **90**, 174411.
16 A. A. Fraerman, O. L. Ermolaeva, E. V. Skorohodov, N. S. Gusev, V. L. Mironov, S. N. Vdovichev and E. S. Demidov, *J. Magn. Magn. Mater.*, 2015, **393**, 452–456.
17 M. V. Sapozhnikov and O. L. Ermolaeva, *Phys. Rev. B: Condens. Matter Mater. Phys.*, 2015, **91**, 024418.
18 C. Heo, N. S. Kiselev, A. K. Nandy, S. Blugel and T. Rasing, *Sci. Rep.*, 2016, **6**, 27146.
19 K. W. Moon, D. H. Kim, S. G. Je, B. S. Chun, W. D. Kim, Z. Q. Qiu, S. B. Choe and C. Y. Hwang, *Sci. Rep.*, 2016, **6**, 20360.
20 Y. Okamura, F. Kagawa, M. Mochizuki, M. Kubota, S. Seki, S. Ishiwata, M. Kawasaki, Y. Onose and Y. Tokura, *Nat. Commun.*, 2013, **4**, 2391.
21 J. V. Kim, F. Garcia-Sanchez, J. Sampaio, C. Moreau-Luchaire, V. Cros and A. Fert, *Phys. Rev. B: Condens. Matter Mater. Phys.*, 2014, **90**, 064410.
22 B. F. Miao, Y. Wen, M. Yan, L. Sun, R. X. Cao, D. Wu, B. You, Z. S. Jiang and H. F. Ding, *Appl. Phys. Lett.*, 2015, **107**, 222402.
23 M. Mruczkiewicz, P. Gruszecki, M. Zelent and M. Krawczyk, *Phys. Rev. B*, 2016, **93**, 174429.
24 K. Tsuruta, M. Mito, H. Deguchi, J. Kishine, Y. Kousaka, J. Akimitsu and K. Inoue, *Phys. Rev. B*, 2018, **97**, 094411.
25 C. Jin, C. Song, J. Wang, H. Xia, J. Wang and Q. Liu, *J. Appl. Phys.*, 2017, **122**, 223901.
26 A. Takeuchi and M. Mochizuki, *Appl. Phys. Lett.*, 2018, **113**, 072404.

27 T. Yokouchi, S. Hoshino, N. Kanazawa, A. Kikkawa, D. Morikawa, K. Shibata, T.-h. Arima, Y. Taguchi, F. Kagawa, N. Nagaosa and Y. Tokura, *Sci. Adv.*, 2018, **4**, eaat1115.

28 *Object oriented micromagnetic framework software (OOMMF)*, online available: http://math.nist.gov/oommf.

29 M. Bi, X. Wang, H. P. Lu, L. Zhang, L. J. Deng and J. L. Xie, *J. Magn. Magn. Mater.*, 2017, **428**, 412–416.

30 M. Garst, J. Waizner and D. Grundler, *J. Phys. D: Appl. Phys.*, 2017, **50**, 293002.

31 M. Beg, M. Albert, M.-A. Bisotti, D. Cortés-Ortuño, W. Wang, R. Carey, M. Vousden, O. Hovorka, C. Ciccarelli, C. S. Spencer, C. H. Marrows and H. Fangohr, *Phys. Rev. B*, 2017, **95**, 014433.

32 M. Mruczkiewicz, M. Krawczyk and K. Y. Guslienko, *Phys. Rev. B*, 2017, **95**, 094414.

33 M. Mruczkiewicz, P. Gruszecki, M. Krawczyk and K. Y. Guslienko, *Phys. Rev. B*, 2018, **97**, 064418.

34 Y. Dai, H. Wang, T. Yang, W. Ren and Z. Zhang, *Sci. Rep.*, 2014, **4**, 6153.